



# A combined in situ time-resolved UV–Vis, Raman and high-energy resolution X-ray absorption spectroscopy study on the deactivation behavior of Pt and Pt–Sn propane dehydrogenation catalysts under industrial reaction conditions

Ana Iglesias-Juez<sup>a</sup>, Andrew M. Beale<sup>a</sup>, Karin Maaijen<sup>a</sup>, Tsu Chien Weng<sup>b</sup>, Pieter Glatzel<sup>b</sup>, Bert M. Weckhuysen<sup>a,\*</sup>

<sup>a</sup> *Inorganic Chemistry and Catalysis, Debye Institute for Nanomaterials Science, Faculty of Science, Utrecht University, 3584 CA Utrecht, The Netherlands*

<sup>b</sup> *European Synchrotron Radiation Facilities, ID26, BP 220, F-38043 Grenoble Cedex, France*

## ARTICLE INFO

### Article history:

Received 10 May 2010

Revised 10 September 2010

Accepted 18 September 2010

### Keywords:

Propane dehydrogenation

Pt–Sn alloy formation

Coke formation

HERFD XANES and Raman

## ABSTRACT

The catalytic performances of Pt/Al<sub>2</sub>O<sub>3</sub> and Pt–Sn/Al<sub>2</sub>O<sub>3</sub> catalysts for the dehydrogenation of propane through consecutive reaction–regeneration cycles have been studied under realistic reaction conditions. A 10-fold successive dehydrogenation–regeneration cycling study, similar to that employed in an industrial propane dehydrogenation reactor, was performed in order to examine the catalyst activity and stability as well as the propene selectivity. Combined in situ UV–Vis/Raman spectroscopy measurements were taken in order to follow the coke formation processes during propane dehydrogenation. This approach allowed correlating propane conversion and propene formation with the on-line determined Raman D over G band intensity ratio and amount of coke formed. These in situ measurements on coke formation and related catalyst deactivation were supplemented by in situ high-energy resolution fluorescence detected (HERFD) XANES measurements in order to characterize the structural and electronic properties of the supported Pt and Pt–Sn nanoparticles during the successive dehydrogenation–regeneration cycles. This combination of powerful spectroscopic techniques revealed unique information regarding the activity behavior and deactivation mechanism of Pt- and Pt–Sn-based propane dehydrogenation catalysts, enabling us to identify important structure–electronic–performance relationships as well as fundamental insight into the dynamics of Pt–Sn alloy formation processes in Pt nanoparticles at elevated temperatures.

© 2010 Elsevier Inc. All rights reserved.

## 1. Introduction

The catalytic dehydrogenation of light alkanes, such as propane, is of great commercial interest due to the growing demand of propene as an important base chemical intermediate [1–4]. Pt-based catalysts have been widely used for alkane dehydrogenation reactions due to their excellent activity [5]. However, this catalyst system suffers from fast deactivation due to coke formation. There are several strategies to improve the catalytic behavior of Pt, including its promotion with a second metal [6,7]. Sn is often added to alter the product distribution for hydrocarbon conversion through the inhibition of hydrogenolysis, isomerisation, cracking and coke formation, thereby enhancing the catalyst selectivity and stability [7,8]. However, the mechanism by which Sn as promoter modifies the catalytic behavior of Pt remains a matter of debate due to the complicated nature of the Pt–Sn alloy system. On the other hand,

even though Sn is one of the most efficient promoters, deactivation due to coke formation is not avoidable and results in catalyst materials still exhibiting short lifetimes. As such, coked catalysts need to undergo a regeneration process (i.e., coke burning) in order to restore the activity. The regeneration treatment typically consists of exposing the coked catalyst to air or oxygen at high temperatures to burn the deposits, followed by a reduction step to bring back the active form of the catalyst (i.e., metallic Pt). Thus, it is important to consider that the exposure of the catalyst material to such oxidation and reduction cycles modifies the catalysts' properties (both structural and electronic), which affects the behavior of the catalysts for subsequent dehydrogenation cycle(s). However, to the best of our knowledge, the majority of literature work mainly concentrates on the characterization of catalyst systems before and after only one dehydrogenation cycle; the study of Padro et al. in which multiple regeneration steps were employed is the only notable exception [9]. Therefore, unfortunately to date, it has not been possible to extract conclusive information regarding the basic principles of catalyst operation/deactivation of this important catalyst system under real reaction conditions.

\* Corresponding author. Fax: +31 30 251 1027.

E-mail address: [b.m.weckhuysen@uu.nl](mailto:b.m.weckhuysen@uu.nl) (B.M. Weckhuysen).

In this work, the catalytic performance of Al<sub>2</sub>O<sub>3</sub>-supported Pt and Pt–Sn catalysts has been investigated and compared for the selective dehydrogenation of propane to propene under industrially relevant conditions. The work makes use of two separate in situ reactor setups: one that utilizes a powder-containing, plug-flow reactor setup that combines on-line activity measurements with the simultaneous recording of in situ UV–Vis and Raman spectroscopy data and a second setup consisting of a flow-through cell using a pressed pellet sample that has been developed so that it is possible to perform catalytic reactions with on-line product monitoring at the outlet (mass spectrometer) while performing in situ high-energy resolution fluorescence detected (HERFD) X-ray absorption spectroscopy (XAS) measurements [10,11]. The results obtained from these innovative real-time characterization studies show a difference in behavior for the catalyst materials (in the presence/absence of Sn as promoter) with regard to both propane dehydrogenation/activation and coke formation (in both the amount and type of coke formed). Differences in the oxidation state and the electronic properties and the local structures of Pt and Sn in Pt–Sn catalysts during successive activation–reaction–regeneration cycles that affect the propane activation mechanism were also followed and have been correlated with the extent of alloy formation. In addition, we observed that during the regeneration process in oxygen to burn-off the formed coke on the catalyst, sintering or segregation of the metals also takes place, causing irreversible deactivation of the catalyst. Based on these new insights, a comprehensive working model for the short- and long-term deactivation of Pt–Sn dehydrogenation catalysts is proposed.

## 2. Materials and methods

### 2.1. Catalyst preparation and physicochemical characterization

A series of Al<sub>2</sub>O<sub>3</sub>-supported Pt and Pt–Sn (Pt: 0.5 wt.% and Sn: 1.5 wt.%) catalysts have been prepared. The proportion of both metals was chosen similar to that employed for Pt–Sn-based industrial catalysts used in the dehydrogenation of propane in order to establish a close correspondence between the model and real systems. The catalyst materials have been synthesized making use of the incipient wet co-impregnation method of a commercial alumina carrier (Norton, 89 m<sup>2</sup>/g). Solutions containing the metal precursors were prepared containing 1.27 g H<sub>2</sub>PtCl<sub>6</sub> (39.96% Pt; Degussa) and 2.91 g SnCl<sub>2</sub>·2H<sub>2</sub>O (Merck, p.a.) diluted in 600 ml ethanol 99.9%. Hundred grams of the carrier material was impregnated with the solution. The ethanol was then evaporated by using a rotavap (50 °C, 20 mbar). The obtained catalyst materials were calcined for 3 h at 560 °C. After propane dehydrogenation, the coke contents of a selection of catalyst samples have been determined using thermogravimetric analysis in artificial air using a Perkin-Elmer Pyris 1 TGA instrument.

### 2.2. In situ X-ray absorption spectroscopy

Experiments at the Sn K edge and Pt L<sub>3</sub> edge during H<sub>2</sub> reduction were conducted using an in situ cell, which allows the investigation of the catalyst materials using X-ray absorption spectroscopy (XAS) for sample temperatures from 25 to 500 °C. This was integrated with a gas flow system in order to switch between different gas atmospheres. EXAFS measurements were taken at the DUBBLE (BM26A) beamline of the European Synchrotron Research Facility (ESRF, Grenoble, France). The beamline was equipped with a double Si(1 1 1) crystal monochromator. Measurements were taken in fluorescence mode using a 9-element germanium detector. The samples were prepared by hand pressing

0.1 g of powder into a self-supporting wafer. This wafer was then placed in a treatment cell and reduced in a flow of 10% H<sub>2</sub> in He for 30 min at 450 °C, the temperature ramp-up rate being 5 °C/min. Afterward, the cell was cooled down and Pt L<sub>3</sub> edge EXAFS scans were acquired at liquid N<sub>2</sub> temperature. Each measurement was repeated two times. The EXAFS data analysis was carried out with the EXCURV program. The EXAFS data were extracted from the averaged absorption spectra through pre-edge subtraction using a modified Victoreen curve and then through background subtraction employing cubic spline routines with a continuously adjustable smoothing factor. Finally, the average spectrum was normalized by dividing the data by the absorption intensity at 50 eV after the edge. The obtained chi ( $\chi$ ) function was analyzed by multiple shells data fitting in *k*-space with a *k*<sup>3</sup>-weighting. From the EXAFS analysis, the obtained first-shell Pt–Pt coordination numbers were used to evaluate the average Pt particle size.

### 2.3. Model calculations for ideal Pt and Pt–Sn nanoparticle geometries

In order to extract particle morphology/bimetal distribution information from the XAFS results, we performed a series of numerical simulations to determine coordination numbers for the first two coordination (Pt and Sn) shells, for different theoretical bimetal particle morphologies. Details on these calculations can be found elsewhere [12]. Bimetal structures were created using the nanocluster building function of the Materials Studio<sup>®</sup> software package based on a Pt unit cell and substituting some Pt atoms for Sn. Various structures were simulated with differing bimetal arrangements including spherical, hemispherical and cubic structures with decorated, core–shell, hemi-sphere and random alloy distributions. The final structures proposed were based on fits (coordination number variability of  $\pm 0.1$ ) to the obtained coordination numbers from the experimental EXAFS analysis.

### 2.4. CO temperature-programmed desorption infrared spectroscopy

Infrared (IR) measurements were taken on self-supporting catalyst wafers ( $\phi = 7$  mm) that were pressed from 0.01 g to 0.02 g of sample material. A pressure of no more than 2 bar was applied during a period of 10 s to prevent the destruction of the pore structure of the support. The wafer was placed in an IR transmission cell equipped with CaF<sub>2</sub> windows. The cell was connected to a gas handling system, which allowed measurements under low pressure (10<sup>−6</sup> bar) as well as under gas flow. The cell was evacuated to 10<sup>−6</sup> bar at 50 °C for 30 min prior to reduction by 60 ml/min flow of H<sub>2</sub> (quality 5.0; Hoekloos). During reduction, the temperature was raised from 50 °C to 450 °C at 3 °C/min and maintained for 30 min at 450 °C. The system was then switched back to vacuum for 30 min at 450 °C, before being cooled down to 50 °C at a rate of 3 °C/min. A first spectrum was taken under vacuum and served as background reference for the catalyst wafer. Next, 10% CO (quality 4.7; Linde AG) in He (quality 4.6; Linde AG) was introduced in the cell until a stable pressure of ca. 0.06 bar was reached. After 30 min of static CO exposure, the cell was evacuated to a pressure of  $2 \times 10^{-6}$  bar for 30 min at 50 °C before Temperature-programmed desorption (TPD) was started by increasing the temperature up to 450 °C at a rate of 3 °C/min. IR spectra were recorded every 2 min on a Perkin-Elmer 2000 FT-IR instrument with an optical resolution of 4 cm<sup>−1</sup> and an accumulation of 25 scans with wavenumbers ranging from 4000 cm<sup>−1</sup> to 1300 cm<sup>−1</sup>. The data acquisition was performed automatically using the Perkin-Elmer Time-Base software. The reproducibility of all IR-TPD measurements was verified by repeating the experiments in two different ways: (1) On two different wafers from the same sample and (2) on the same wafer by applying the same procedure two times in a row without opening the IR cell. Band positions and

corresponding area data were estimated from the baseline-corrected spectra using the Perkin-Elmer Time-Base<sup>®</sup> software package.

### 2.5. Catalytic activity and coke formation measurements

The catalytic activity testing was carried out in an in situ combined UV-Vis/Raman setup with on-line gas chromatography (GC) analysis. Details of this experimental setup can be found elsewhere [11]. A cylindrical quartz reactor with a square section which was made out of optical grade quartz windows was placed in an oven; the optical grade windows allow for the collection of high-quality Raman and UV-Vis data. A Kaiser Optical Systems Inc. Raman spectrometer was placed on one side of the reactor. Spectra were recorded in Holograms 4.0 with an exposure time of 7 s and 11 accumulations. On the other side of the reactor, a high-temperature UV-Vis probe was positioned detecting every 2 min (5 s, 10 accumulations) in situ UV-Vis spectra. Since the reflectance properties of the catalyst material (i.e., catalyst darkening) changed during the reaction due to the formation of coke on the catalyst, a correction on the observed Raman intensity was made by UV-Vis. Details of this procedure can be found elsewhere [13]; 0.5 g of catalyst was placed in the reactor as packed bed on quartz wool. A variable gas feed was introduced in the reactor. The quantification of the gas products was possible by an on-line Interscience compact GC equipped with two detectors, namely a FID and TCD with a Porabond-Q and a Carboxan column, respectively. At the outlet of the reactor, the gas stream was diluted with He for GC analysis. Chromatograms were acquired every 5 min. Different conditions were employed for the activity measurements:

- Pre-treatment: The samples were pre-activated in the same reactor before C<sub>3</sub>H<sub>8</sub> dehydrogenation reaction was carried out. A H<sub>2</sub> flow (9.5 ml min<sup>-1</sup>) was introduced, while the temperature was increased from room temperature up to 590 °C with a temperature ramp of 10 °C min<sup>-1</sup>. After the reduction, the reactor was purged with He for 5 min.
- Dehydrogenation reaction: After reduction, a gas stream of pure propane (9 ml min<sup>-1</sup>) humidified with 9 v/v% of steam was introduced in the reactor. The reaction proceeded for 6 h at 590 °C, and after this treatment, the system was purged with He for 5 min.
- Regeneration process: The sample was regenerated at the same temperature in an oxygen environment to burn the coke from the catalyst material. The regeneration process consisted of a moderate reoxidation in 7% of O<sub>2</sub> for 1 h and a more severe reoxidation in 20% of O<sub>2</sub> at 590 °C. After this time, no CO<sub>2</sub> was detected in the GC, which suggests that the burn-off of the coke was complete. The system was purged with He for 5 min.
- Re-activation of the catalyst: Without modifying the temperature, a reduction step was first performed to activate the catalyst material. This time a gas flow of 20% of H<sub>2</sub> in He was used. After a He purge, the dehydrogenation reaction was started again and considered as a new cycle. This cycle was repeated 10 times and after the reactor was cooled down in He to RT.

### 2.6. In situ high-energy resolution fluorescence detected X-ray absorption spectroscopy

Measurements were taken at the ID26 beamline of ESRF (Grenoble, France). High-energy resolution fluorescence detected (HERFD) X-ray absorption spectroscopy (XAS) at the L<sub>3</sub> (11.5637 keV) edges was performed on the Pt/Al<sub>2</sub>O<sub>3</sub> and Pt–Sn/Al<sub>2</sub>O<sub>3</sub> catalysts under the same gas conditions and reaction temperatures as discussed above for the combined in situ UV-Vis/Raman spectroscopy

measurements. For these HERFD-XAS measurements, we used the horizontal plane Rowland circle spectrometer tuned to the Pt L<sub>α1</sub> (9.442 eV) fluorescence line. The (660) Bragg reflection of four spherically bent Ge wafers with R = 1 m and a diameter of 89 mm was required. Approximately, 40 mg of catalyst was pressed to a self-supporting wafer, which fits in the sample holder.

An in situ cell provided by the Sample Environment Support Service (SESS) of the ESRF was used. It is specially designed for the use of pelleted samples and allows for the measurement of fluorescence data [10]. The maximum working temperature can go up to 1000 °C. The gas cell included cooling loops, thermal couples and heaters all built-in. It was also equipped with a gas flow control (from the ID26 ESRF beamline) to use different gas atmosphere. The experimental runs consist of an in situ pre-reduction at 600 °C (20% H<sub>2</sub>/He) followed by continuous propane dehydrogenation (10% C<sub>3</sub>H<sub>8</sub>/He) until the temperature reaches 600 °C. Then, subsequent step changes in the gas mixture under isothermal conditions were applied; i.e., cycles of propane dehydrogenation (10% C<sub>3</sub>H<sub>8</sub>/He), regeneration in O<sub>2</sub> atmosphere and re-reduction in H<sub>2</sub>, similar to the catalytic study described above. An on-line mass spectrometer provided a measure of the global catalytic process at hand through monitoring the composition of the gaseous feedstock, ensuring reproduction, on the ESRF beamline of a reaction environment and of catalytic performances similar to those present in the in situ UV-Vis/Raman setup described above.

## 3. Results and discussion

### 3.1. Catalytic activity studies of supported Pt and Pt–Sn nanoparticles

Fig. 1 shows an overview of the catalytic performances of the Pt and Pt–Sn/Al<sub>2</sub>O<sub>3</sub> catalyst materials during 10 successive dehydrogenation–regeneration cycles. Although the fresh Pt/Al<sub>2</sub>O<sub>3</sub> catalyst exhibits the highest initial reaction activity, after 6 h of reaction, the catalyst deactivates very fast with propane conversions decreasing from 40% to 5%. After this first reaction and subsequent isothermal regeneration process, the catalytic activity is observed to be much lower during the second and third reaction cycles, resulting in almost no net conversion after three dehydrogenation–regeneration cycles.

In contrast, the presence of Sn as a promoter drastically improves the catalytic behavior. The Pt–Sn/Al<sub>2</sub>O<sub>3</sub> catalyst material possesses both a higher propane conversion and propene selectivity, which is maintained throughout the duration of the first dehydrogenation step. As with the Pt/Al<sub>2</sub>O<sub>3</sub> catalyst, a decrease in the catalytic activity is also observed after the first regeneration treatment. However, this happens more gradually than for the Pt/Al<sub>2</sub>O<sub>3</sub> catalyst. Further deactivation occurs during subsequent dehydrogenation–regeneration cycles although a steady state is reached after 5–6 cycles. Interestingly, despite this gradual catalyst deactivation, the net conversion during the experiment is always higher for the Pt–Sn/Al<sub>2</sub>O<sub>3</sub> catalyst than for the Pt/Al<sub>2</sub>O<sub>3</sub> catalyst. This is illustrated in Fig. 1A.

The corresponding propene selectivities of the Pt/Al<sub>2</sub>O<sub>3</sub> and Pt–Sn/Al<sub>2</sub>O<sub>3</sub> catalysts are shown in Fig. 1B. It is clear that for the fresh Pt/Al<sub>2</sub>O<sub>3</sub> catalyst, the propene selectivity decreases with reaction time. However, in contrast, the Pt–Sn/Al<sub>2</sub>O<sub>3</sub> catalyst not only shows higher overall propene selectivity, but also the selectivity increases gradually throughout the experiment. After the first regeneration process, the Pt–Sn/Al<sub>2</sub>O<sub>3</sub> catalyst still presents high selectivity, which remains constant during the cycle. Nevertheless, for the following dehydrogenation cycles, a decrease in selectivity was observed during the reaction time which became more acute after 5–6 cycles. The hydrocarbon distribution for the Pt/Al<sub>2</sub>O<sub>3</sub> and Pt–Sn/Al<sub>2</sub>O<sub>3</sub> catalysts during the multiple reaction cycles is

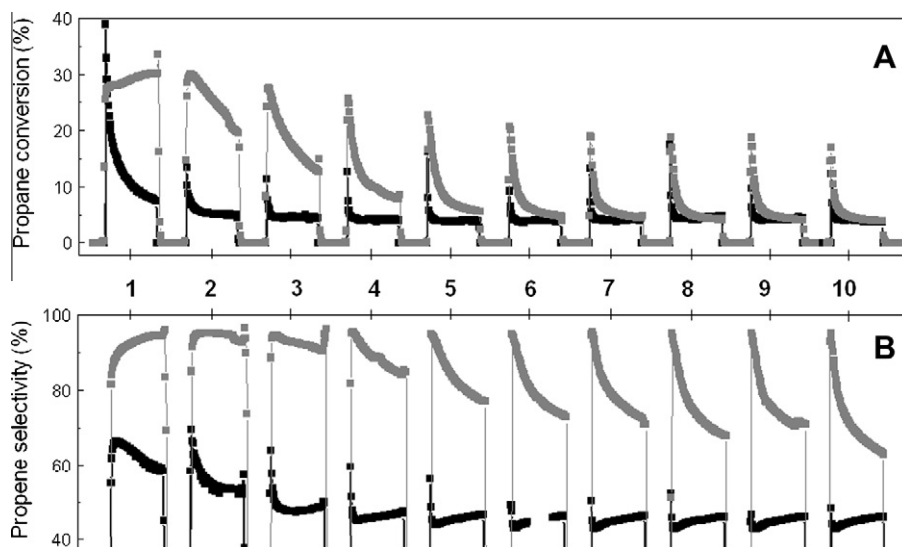


Fig. 1. (A) Propane conversion and (B) propene selectivity of (■) Pt and (□) Pt–Sn/Al<sub>2</sub>O<sub>3</sub> catalysts during 10 consecutive dehydrogenation–regeneration cycles at 590 °C.

given in Fig. S1, indicating that besides propene also ethane, ethene and some methane are formed.

### 3.2. Analysis of coke deposit formation and its relation to catalyst performance

The amount of coke deposited on the catalyst materials after propane dehydrogenation for 6 h was measured by using thermogravimetric analysis. The amount of coke on the Pt/Al<sub>2</sub>O<sub>3</sub> and Pt–Sn/Al<sub>2</sub>O<sub>3</sub> catalysts was 8.2 and 7.3% w/w, respectively. The formation of coke on a Pt–Sn/Al<sub>2</sub>O<sub>3</sub> catalyst was only a bit lower than on a Pt/Al<sub>2</sub>O<sub>3</sub> catalyst; however, the influence on the propane dehydrogenation activity and propene selectivity appears to be much more significant and merited a more detailed spectroscopic investigation of the coke formed.

As a result, we have on-line monitored the formation of coke during propane dehydrogenation using a combined in situ UV–Vis/Raman setup. The in situ UV–Vis spectra were used to perform a correction of the decrease in the Raman signal caused by the darkening of the catalyst as coke deposits gradually formed on the catalyst surface. Detailed information about this procedure can be found elsewhere [13], and the coke amount from the TGA analysis was used to quantify the in situ Raman data. As an example, Fig. 2 shows the raw in situ Raman spectra for the Pt/Al<sub>2</sub>O<sub>3</sub> catalyst during the first propane dehydrogenation cycle measured at 590 °C.

Two distinct Raman bands at around 1584 and 1321 cm<sup>−1</sup> were observed. These Raman bands can be ascribed to coke G and D modes, respectively. Single crystal graphite has a single Raman active mode, (the zone-center mode) at 1580 cm<sup>−1</sup> of E<sub>2g</sub> symmetry and is labeled ‘G’ for ‘graphite’. Disordered graphite has a second mode around 1350 cm<sup>−1</sup> of A<sub>1g</sub> symmetry labeled ‘D’ for ‘disorder’. It corresponds to a breathing vibration of rings at the K zone boundary [14,15]. An unusual and significant fact is that the Raman spectra of most disordered carbons remain dominated by these two G and D modes of graphite, even when the carbons do not have a particular graphitic ordering [16]. The G mode is actually the stretching vibration of any pair of sp<sup>2</sup> sites, whether in C=C chains or in aromatic rings [16]. This mode is then also seen in ethylene as well as in graphite but is blue-shifted to higher wavenumbers. Thus, G in this instance does not only mean ‘graphite’. The D mode is the breathing mode of those sp<sup>2</sup> sites only in rings, not in chains. Therefore, these bands provide information not only on the

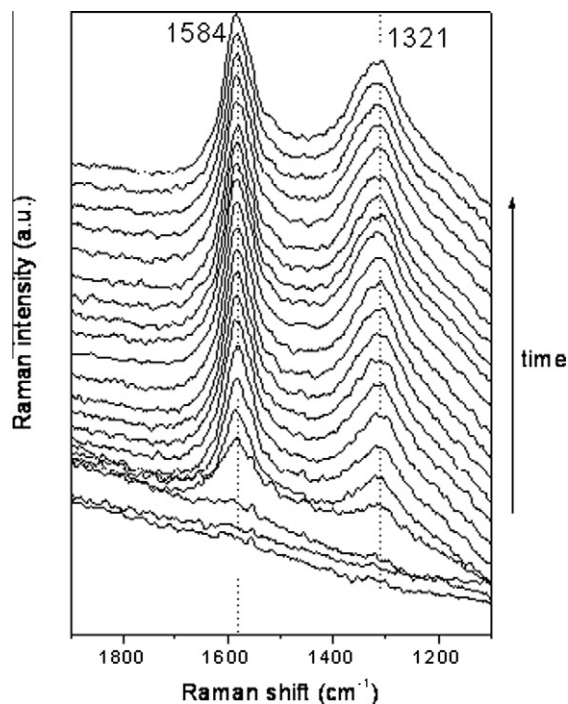


Fig. 2. In situ Raman spectra of the Pt/Al<sub>2</sub>O<sub>3</sub> catalyst acquired along the first dehydrogenation of propane cycle for 6 h at 590 °C.

amount of coke present on the catalyst, but also on its nature. Ferrari and Robertson [16] found that it is possible to classify the Raman spectra of carbons, using the intensity ratio of the D and G bands, within a three-stage model of disorder degree as follows: (1) sp<sup>3</sup> amorphous carbons (a-C) to sp<sup>2</sup> a-C, (2) a-C sp<sup>2</sup> to nano-crystalline graphite and (3) nano-crystalline graphite to more perfect graphite.

The Raman intensity profile of the coke band located at 1584 cm<sup>−1</sup> after UV–Vis correction is shown in Fig. S2. It was noted that the amount of coke in the Pt/Al<sub>2</sub>O<sub>3</sub> and Pt–Sn/Al<sub>2</sub>O<sub>3</sub> catalysts gradually increases during propane dehydrogenation, but after regeneration treatment the total amount of coke decreases in the successive cycles. This behavior parallels the propane conversion profiles. For the Pt–Sn/Al<sub>2</sub>O<sub>3</sub> catalyst, the presence of Sn not only

reduces the amount of coke formed during a propane dehydrogenation run but also modifies its rate of formation.

The intensity ratio of the D and G Raman bands at around 1321 and 1584  $\text{cm}^{-1}$ , respectively, provides information on the type of coke that is formed on the surface. The results are displayed in Fig. 3 for cycle 1, 2 and 10, together with the activity data for the Pt/Al<sub>2</sub>O<sub>3</sub> and Pt–Sn/Al<sub>2</sub>O<sub>3</sub> catalysts. For Pt/Al<sub>2</sub>O<sub>3</sub>, an initial D over G ratio of 0.4 is observed. This ratio increases with time on stream until reaching a value of around 1 where it remains constant even after one hour of reaction. These results suggest that at the beginning of the catalytic reaction, a more disordered aliphatic type of coke forms and after 1 h the amount of coke increases but without changing its nature. A similar trend is observed in the following additional propane dehydrogenation cycles. In the case of the Pt–Sn/Al<sub>2</sub>O<sub>3</sub> catalyst, the initial D over G ratio is around 0.7 and remains almost constant during the cycle, indicating that no changes take place in the nature of the coke. However, after the first regeneration process, the coke formed at the beginning of the next dehydrogenation cycle seems more disordered and with reaction time, the D over G ratio first increases, but after one hour-on-stream the D over G ratio decreases. This indicates that the nature of coke becomes more graphitic; the propene would initially form oligomers (or polymers) and aromatics, but after a while, these surface species would lose hydrogen and become more graphitic. Fig. 3 also shows that the change in the nature of the coke deposits coincides with a maximum in propane conversion. Apparently, then the type of coke influences the activity of the propane dehydrogenation reaction. In the 10th dehydrogenation cycle, the same behavior is observed showing a clear relation between the deactivation of the catalyst material and the formation of more graphitic coke.

The Pt/Al<sub>2</sub>O<sub>3</sub> catalyst exhibits a higher initial propane conversion than the Pt–Sn/Al<sub>2</sub>O<sub>3</sub> catalyst. However, the initial selectivity

to propene is much lower (~60%) when compared to the Pt–Sn/Al<sub>2</sub>O<sub>3</sub> catalyst (~90%) (Fig. 1B). The high selectivity toward cracking products, namely methane and ethane, for the Pt/Al<sub>2</sub>O<sub>3</sub> catalyst, as illustrated in Fig. S1, indicates that the supported Pt nanoparticles in this catalyst are very active for C–C bond activation [17–19]. From the above observation, it can be suggested that a reaction mechanism involving common surface intermediates, which form activated/partially dehydrogenated propane, can either desorb as C<sub>3</sub>H<sub>6</sub> or further undergo cracking to C<sub>1</sub>, C<sub>2</sub> and even to surface carbon deposits. The fast decrease in conversion points to a rapid deactivation of the catalyst probably caused by the blocking of active Pt sites by coke formation.

During the first dehydrogenation cycle, the Pt–Sn/Al<sub>2</sub>O<sub>3</sub> catalyst shows lower initial propane conversion and a higher rate of coke formation when compared to the Pt/Al<sub>2</sub>O<sub>3</sub> catalyst. In the presence of Sn, the light products that are produced are ethane and methane in equimolar amounts, which is typical for a metal-catalyzed hydrogenolysis reaction (Fig. S1). The selectivity to light products is much lower and decreases with time, suggesting that the hydrogenolysis reaction is inhibited by coke formation on the metal particles [7]. However, despite the amount of coke formed, Pt–Sn/Al<sub>2</sub>O<sub>3</sub> exhibits a much higher selectivity to propene and the amount of propene increases together with propane conversion with time on stream, displaying better catalyst stability than the Pt/Al<sub>2</sub>O<sub>3</sub> catalyst.

The results indicate that the presence of Sn not only modifies the electronic properties of the Pt nanoparticles and therefore the activation of propane but also produces a ‘drain-off’ effect. This drain-off effect keeps the Pt sites clean by removing the coke precursors from the vicinity of active sites to the support. This hypothesis was first proposed by Lieske et al. and has been discussed in the context of a particle ensemble effect [20]. It suggests that coke precursors such as olefinic species adsorb less strongly on the

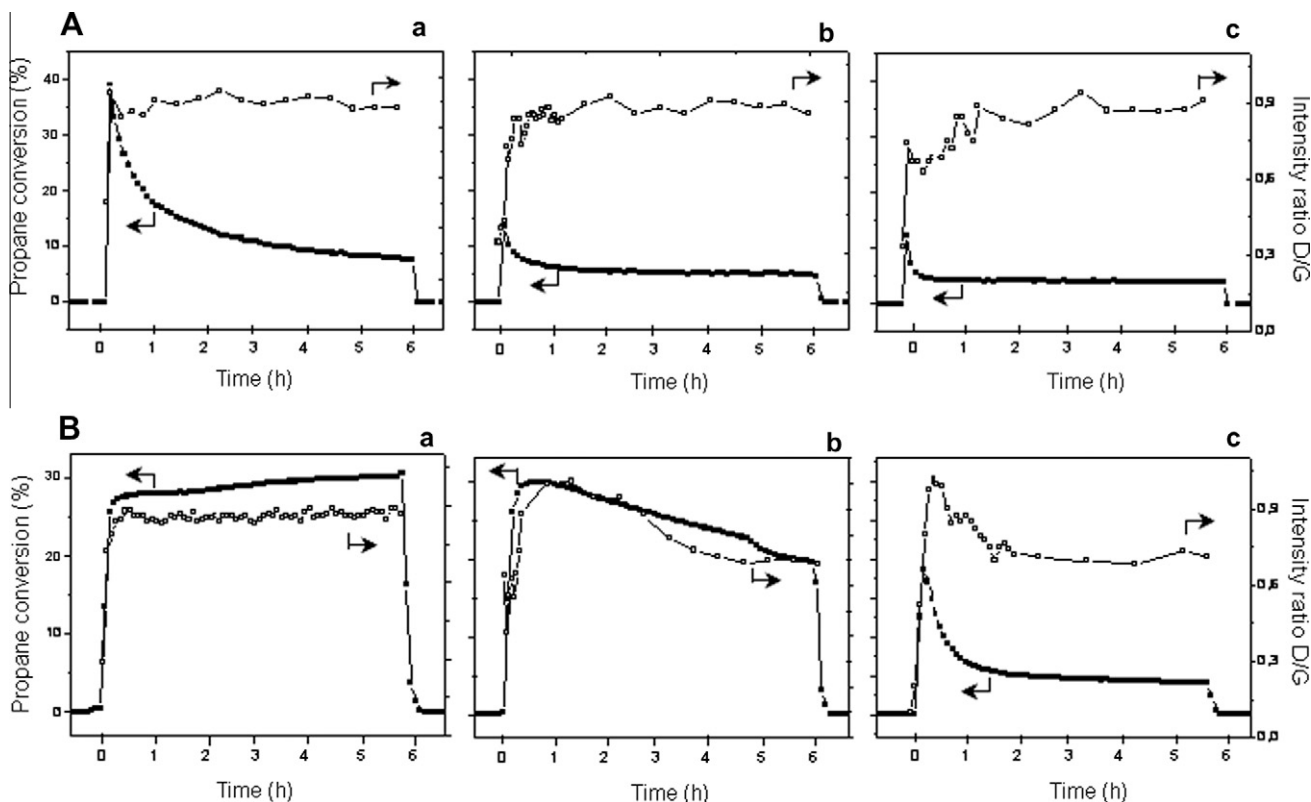


Fig. 3. Intensity ratio of the D and G Raman bands (□) and propane conversion (■) during cycle (a) 1, (b) 2 and (c) 10 of propane dehydrogenation for the (A) Pt/Al<sub>2</sub>O<sub>3</sub> and (B) Pt–Sn/Al<sub>2</sub>O<sub>3</sub> catalyst materials.

Pt–Sn bimetallic catalyst due to an ensemble effect of Sn. Therefore, coke precursors are mobile and easily migrate to the support where they finally deposit as coke. In recent work, Kumar et al. [21] proposed a ‘modified drain-off’ effect, which is based on a combination of the electronic and drain-off effects. After one regeneration process, although the Pt/Al<sub>2</sub>O<sub>3</sub> catalyst exhibits lower propane conversion, the same catalytic behavior and coke evolution is observed. On the other hand, the Pt–Sn/Al<sub>2</sub>O<sub>3</sub> catalyst material possesses both different activity and different coke formation with respect to the initial dehydrogenation cycle, which suggests a modification of the properties of the active sites.

### 3.3. Electronic and structural characterization of Pt and Pt–Sn nanoparticles

#### 3.3.1. XANES-EXAFS analysis

The normalized L<sub>3</sub> XANES spectra obtained for the Pt/Al<sub>2</sub>O<sub>3</sub> catalyst after H<sub>2</sub> reduction display a characteristic Pt(0) spectrum with the same edge position as a Pt foil reference. However, while the spectrum shape of the Pt–Sn/Al<sub>2</sub>O<sub>3</sub> catalyst also resembles that of the Pt foil, the absorption edge is shifted to higher energy (Fig. S3). This points to a clear electronic interaction between the Sn and Pt and in particular that Sn withdraws electron density from Pt. Also a clear red shift is visible for the 5f Continuum Resonance (CR), located at ca. 11,592 eV, with respect to the Pt/Al<sub>2</sub>O<sub>3</sub> sample (Fig. S3). This red shift indicates an increase in the Pt–Pt nearest distance most likely associated with the dissolution of Sn atoms in the Pt fcc structure and the incipient formation of an alloy phase [22].

The Sn K edge was also measured during H<sub>2</sub> treatment. XANES analysis shows that Sn is presented initially as SnO<sub>2</sub> and reduction to SnO takes place during the ramp of temperature in H<sub>2</sub> (Fig. S4). From Pt XAS results, it is clear that an interaction between both metals exists and Pt–Sn alloy formation is detected. However, it is not possible to extract the same conclusions from Sn K edge data, as X-ray absorption is a bulk technique and there are three times more Sn than Pt in the sample and EXAFS results for Pt indicates that only a small fraction of Sn comes into the alloy. Therefore, it is not possible to distinguish this phenomenon of alloy formation in the data from Sn K edge as for the most part SnO is detected.

Coordination numbers obtained from the EXAFS analysis (more details presented in the Supporting information, see Figs. S5 and S6) provide an indication of the Pt particle size, and Table 1 summarizes the coordination numbers of the Pt/Al<sub>2</sub>O<sub>3</sub> and Pt–Sn/Al<sub>2</sub>O<sub>3</sub> catalysts. From the Fourier transforms, it can be concluded that no peak is present corresponding to a Pt–O shell in any of the samples, indicating that there are no detectable oxygen atoms in the first coordination shell of Pt in the catalyst. This confirms the complete reduction of Pt in all the samples. A Pt–Pt coordination number of  $N = 7.7$  in the Pt/Al<sub>2</sub>O<sub>3</sub> catalyst indicates that if the catalyst is predominantly homogeneous, there are 50–55 atoms in the Pt nanocluster [12,23]. It is clear that the addition of Sn decreases the particle size of the Pt nanoclusters as lower coordination numbers are obtained for the Pt–Sn/Al<sub>2</sub>O<sub>3</sub> catalyst material. Moreover, for the Pt–Sn/Al<sub>2</sub>O<sub>3</sub> catalyst, it is necessary to introduce another

coordination shell, namely Pt–Sn, at similar distances as the Pt–Pt first shell ( $R = 2.76$  Å) to obtain a good fit to the data. The presence of this Pt–Sn coordination shell is evidence for the existence of a Pt–Sn alloy in the catalyst.

From Table 1, it can be concluded that the Pt particle size increases throughout the whole experiment for the Pt/Al<sub>2</sub>O<sub>3</sub> catalyst. This is also observed for the Pt–Sn/Al<sub>2</sub>O<sub>3</sub> catalyst, which also shows an increase in the degree of Pt–Sn alloying after more dehydrogenation–regeneration cycles. But it is clear that the presence of Sn results in a decrease in the particle size of the Pt when compared to the Pt/Al<sub>2</sub>O<sub>3</sub> catalyst system. Moreover, in the Pt–Sn/Al<sub>2</sub>O<sub>3</sub> catalyst after 1 and 10 cycles, the Pt–Sn entities differ in the amount of Sn in the alloy and a progressive Sn enrichment is observed.

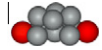
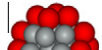
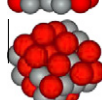
In order to determine the distribution of Pt and Sn in the bimetallic structure for the Pt–Sn/Al<sub>2</sub>O<sub>3</sub> catalyst at the different stages: fresh, after 1 and 10 cycles, a series of models were created where the influence of the bimetal distribution on the coordination number for the first two coordination shells was examined. These simulations helped us to propose possible particle morphologies based on the EXAFS. They are summarized in Table 2. The EXAFS results suggest the formation of 11 atom semispherical-like nanoparticles, for the fresh Pt–Sn/Al<sub>2</sub>O<sub>3</sub> catalyst, which is poor in Sn. More specifically, the Sn atoms are located at the surface of these Pt nanoparticle entities. After one dehydrogenation–regeneration cycle, both the Pt nanoparticle size and the Sn content in the Pt–Sn alloy increase but this time resulting in the formation of a core–shell type structure where Sn is located in the outer layer. However, after 10 successive dehydrogenation–regeneration cycles, not only the number of Sn atoms increases, but also their dilution in the whole Pt nanoparticles. These effects give rise to more homogeneous bimetallic entities.

#### 3.3.2. CO-TPD IR analysis

The CO desorption curves shown in Fig. 4 indicate that the addition of Sn decreases the initial amount of CO adsorbed on the Pt nanoparticles and also that these surface species desorb at lower temperatures. To understand this observation, both particle size and electronic effects have to be taken into account. As discussed above, Sn decreases the Pt particle size and thus creates more centers on the surface available for CO adsorption. However, the lower amount of CO observed here suggests that Sn partially covers those centers as observed in our predicted models based on the EXAFS analysis. On the other hand, Pt sites in the Pt–Sn alloy are more electron deficient since Sn draws electron density away from Pt. Therefore, the adsorption properties of Pt are also modified by the presence of Sn: the more electron-poor Pt species adsorb CO more weakly and, as a consequence, COads species desorb at lower temperatures. This is exactly what we observe in Fig. 4.

**Table 2**

Theoretical coordination numbers (CN) and calculated morphologies, number of atoms (NT) and shape, for the Pt–Sn alloy nanoparticles in a Pt–Sn/Al<sub>2</sub>O<sub>3</sub> catalyst in the fresh state and after 1 and 10 dehydrogenation–regeneration cycles.

	Pt–Sn/Al <sub>2</sub> O <sub>3</sub>				Morphology
	CN <sub>Pt–Pt</sub>	CN <sub>Pt–Sn</sub>	NT <sub>Pt</sub>	NT <sub>Sn</sub>	
Fresh	4.44	0.67	9	2	
After 1 cycle	4.96	2.04	16	10	
After 10 cycles	3.43	4.10	22	16	

**Table 1**

Pt–Pt and Pt–Sn coordination numbers (CN) from a first-shell EXAFS analysis for reduced Pt/Al<sub>2</sub>O<sub>3</sub> and Pt–Sn/Al<sub>2</sub>O<sub>3</sub> catalysts. See all fitting details in Table S1 in the Supporting information.

	Fresh		After 1 cycle		After 10 cycles	
	CN <sub>Pt–Pt</sub>	CN <sub>Pt–Sn</sub>	CN <sub>Pt–Pt</sub>	CN <sub>Pt–Sn</sub>	CN <sub>Pt–Pt</sub>	CN <sub>Pt–Sn</sub>
Pt/Al <sub>2</sub> O <sub>3</sub>	7.7	–	8.0	–	9.6	–
Pt–Sn/Al <sub>2</sub> O <sub>3</sub>	4.4	0.7	5.0	2.1	3.4	4.0

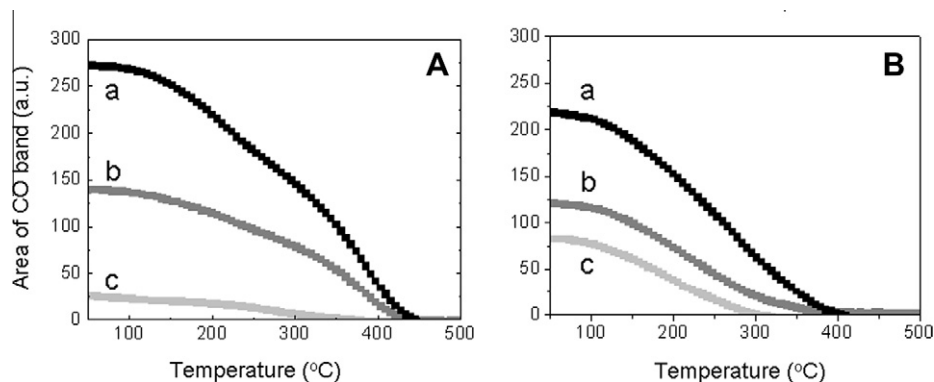


**Fig. 4.** Desorption profiles obtained from CO-TPD IR experiments on (A) Pt/Al<sub>2</sub>O<sub>3</sub> and (B) Pt–Sn/Al<sub>2</sub>O<sub>3</sub> samples: (a) fresh, (b) after 1 dehydrogenation–regeneration cycle and (c) 10 dehydrogenation–regeneration cycles.

The CO desorption measurements on the samples that had undergone 1 and 10 dehydrogenation–regeneration cycles, as also given in Fig. 4, show that the amount of adsorbed CO decreases after consecutive cycles, most likely due to the increase in particle size leading to a lower number of adsorption sites on the surface. The presence of Sn reduces sintering during regeneration so that the decreasing amount of CO adsorption is lower. An increase in particle size of Pt–Sn entities after 1 and 10 cycles is also observed (Table 1), but the differences in the amount of adsorbed CO can be also ascribed to the Sn enrichment of the Pt–Sn alloy after 10 cycles, covering more sites on the surface. This Sn enrichment could also explain why CO desorbs at lower temperatures after the 10 cycles experienced by the Pt–Sn catalyst.

Table 3 summarizes the CO stretching frequencies observed for the Pt and Pt–Sn/Al<sub>2</sub>O<sub>3</sub> samples. A red shift in the CO stretching frequency for the Pt–Sn/Al<sub>2</sub>O<sub>3</sub> catalyst is seen when compared to the Pt/Al<sub>2</sub>O<sub>3</sub> catalyst. The position of the adsorbed CO band is affected by both geometric and electronic effects [24,25]. Since Sn reduces the particle size, a lower CO stretching frequency would be expected as increasing the number of under-coordinated sites (e.g. edges and corners), results in stronger sites for CO adsorption. On the other hand, Sn withdraws charge from Pt as was concluded from the shift to higher energies of the XANES edge in the spectrum of the Pt–Sn/Al<sub>2</sub>O<sub>3</sub> catalyst (Fig. S3), and therefore, a shift to a higher frequency is anticipated. Since a shift toward lower wavenumbers is observed, the structural effect must predominate. In Table 3, the change in the CO band position is also shown for the Pt/Al<sub>2</sub>O<sub>3</sub> and Pt–Sn/Al<sub>2</sub>O<sub>3</sub> catalysts after 1 and 10 dehydrogenation–regeneration cycles. As the Pt particle size of the Pt/Al<sub>2</sub>O<sub>3</sub> catalyst increases after the dehydrogenation and regeneration process (Table 1), it was expected that the CO stretching frequency would increase [24]. However, a gradual decrease is seen as the catalyst undergoes more cycles (Table 3).

These observations indicate that the change in particle size modifies the interaction between Pt and CO, suggesting a modification in the Pt adsorption properties which may be due to changes in the interaction with the support. In the Pt–Sn/Al<sub>2</sub>O<sub>3</sub> catalyst, the

particle size after 1 cycle is smaller than in the Pt/Al<sub>2</sub>O<sub>3</sub> catalyst; however, an increase in the CO stretching frequency is detected. This is consistent with Sn preferentially locating at highly coordinatively unsaturated surface Pt sites as the EXAFS results suggest (Table 2). Consequently, the degree of unsaturation in the coordination sphere of Pt sites decreases, while the interactions between Pt and Sn increase. This results in a modification of the electronic properties and therefore the catalytic properties of Pt.

#### 3.4. Study of the Pt and Pt–Sn nanoparticles activation during H<sub>2</sub> reduction

Fig. 5A shows the intensity contour map of the HERFD XANES spectra acquired of the Pt/Al<sub>2</sub>O<sub>3</sub> catalyst during the ramp of temperature up to 600 °C under a H<sub>2</sub> flow. It can be concluded that Pt is initially present as an oxidic Pt phase. During the H<sub>2</sub> treatment at elevated temperatures, the edge shifts to lower energies and the intensity of the rising absorption edge decreases, indicating that the reduction in the Pt species takes place at ca. 140–210 °C leading to the formation of metallic Pt (Fig. 5B).

In the case of the Pt–Sn/Al<sub>2</sub>O<sub>3</sub> catalyst (Fig. 6A), the reduction process starts at a similar temperature, resulting in the eventual formation of Pt(0), but at intermediate temperatures (at ca. 210–350 °C) a new species is observed, which is evidence for the formation of a Pt–Sn alloy. By increasing the temperature, the total reduction in Pt took place including the insertion of Sn into the structure and consequent formation of a Pt–Sn alloy (Fig. 6B) [23].

#### 3.5. Analysis of the Pt–hydrocarbon interaction

The intensity contour map of the HERFD XANES spectra for the Pt/Al<sub>2</sub>O<sub>3</sub> and Pt–Sn/Al<sub>2</sub>O<sub>3</sub> catalysts acquired during the ramp of temperature up to 600 °C under propane flow is displayed in Fig. S8. Addition of propane to the Pt-containing catalysts after H<sub>2</sub> reduction induces changes in the XANES spectra. To emphasize these changes in the spectra, L<sub>3</sub> Δμ difference spectra were taken, with the spectrum of the bare metal measured at the same temperature used as a reference [26,27]. These Δμ difference spectra for the Pt/Al<sub>2</sub>O<sub>3</sub> catalyst at 100, 140 and 400 °C are shown in Fig. 7A. The propane-induced effect at 100 °C manifests itself as a narrow negative feature at 11,563 eV and a broader positive peak at 11,567 eV. The negative peak is a result of an edge shift to higher energies, whereas the positive feature is due to an enhanced intensity in the white-line that is broadened on the high-energy side. When the temperature increases, the intensity of these features became enhanced. A maximum in intensity is reached around 140 °C and after that they both decrease and the contribution around 11,567 eV shifts slightly to lower energies.

**Table 3**  
IR stretching frequency of CO adsorbed on reduced Pt/Al<sub>2</sub>O<sub>3</sub> and Pt–Sn/Al<sub>2</sub>O<sub>3</sub> catalysts.

	Pt/Al <sub>2</sub> O <sub>3</sub>	Pt–Sn/Al <sub>2</sub> O <sub>3</sub>
	CO stretching frequency (cm <sup>-1</sup> )	
Fresh	2061	2051
After 1 cycle	2062	2083
After 10 cycles	2047	2048

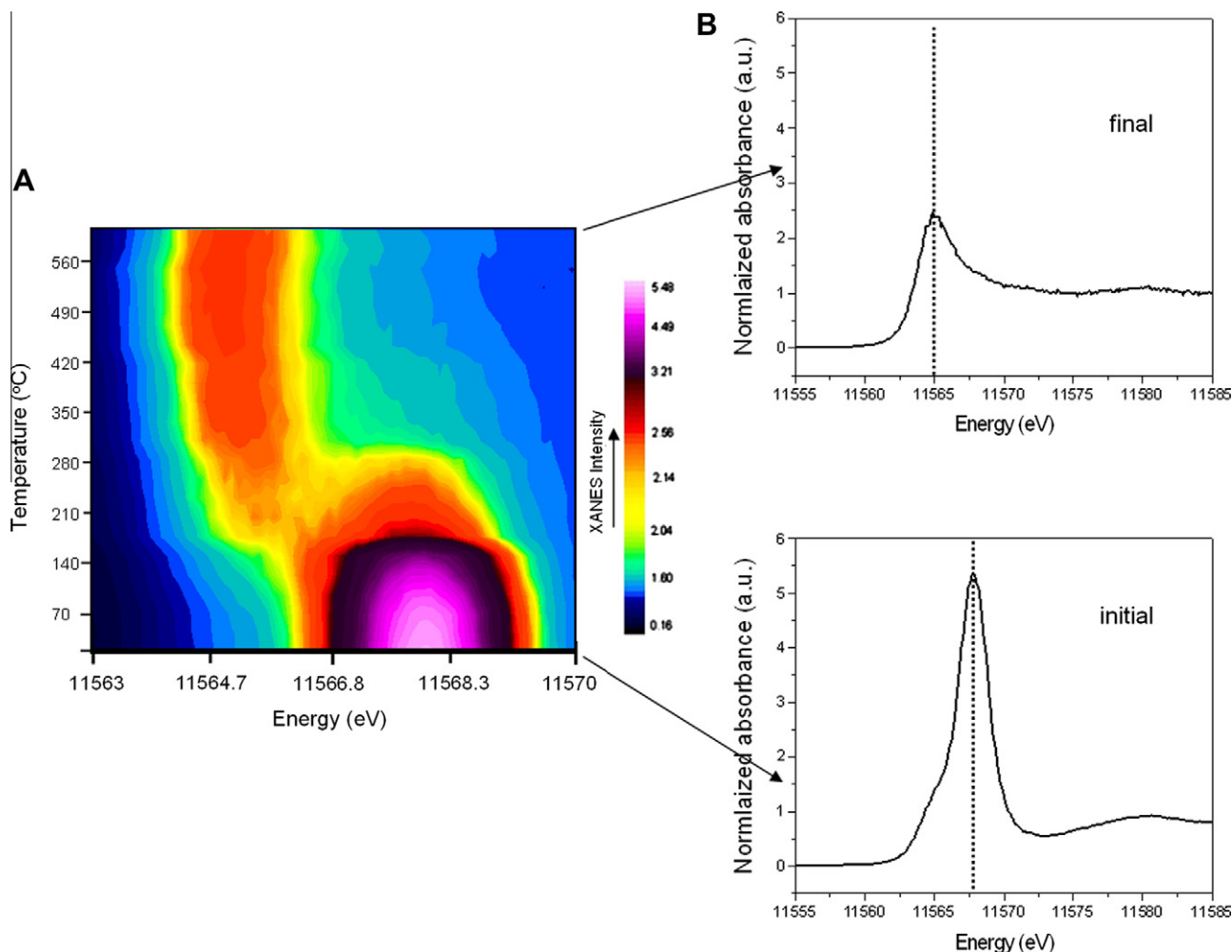


**Fig. 5.** (A) Intensity contour map of the HERFD XANES spectra of a Pt/Al<sub>2</sub>O<sub>3</sub> catalyst acquired during the ramp of temperature up to 600 °C under a H<sub>2</sub> flow and (B) selection of HERFD XANES spectra of the initial and final Pt species formed in the catalyst material.

The L<sub>3</sub> Δμ spectra for the Pt–Sn/Al<sub>2</sub>O<sub>3</sub> catalyst upon exposure to propane are shown in Fig. 7B. The change in the spectra is clearly different from those of the Pt/Al<sub>2</sub>O<sub>3</sub> catalyst as a shift in the edge position of the spectra to lower energies is observed. As a result, the negative feature around 11,563 eV seen for the Pt/Al<sub>2</sub>O<sub>3</sub> catalyst is not observed and at the same energies a positive contribution was detected, overlapping with a peak centered around 11,567 eV. A new very broad yet negative contribution is also observed between 11,570 and 11,578 eV. When the temperature rises, the intensity of those positive peaks increases and after 120 °C they diminish before shifting to lower energies.

The addition of propane to both catalysts induces changes in the Pt L<sub>3</sub> white-line, indicating changes in the electronic structure that result from the bonding of propane to the metal. We summarize that the overall dehydrogenation reaction probably involves three major steps: (i) cleavage of the first C–H bond in a dissociative adsorption step, resulting in an adsorbed propyl group; (ii) cleavage of the second C–H bond, resulting in a π- or σ-bonded olefin; (iii) desorption of the olefin. The differences between pure Pt itself and the Pt–Sn alloy, manifested in the shape of the XANES spectra, suggest a difference in the types of interaction of the hydrocarbon on the Pt surfaces [28,29].

In the case of the Pt/Al<sub>2</sub>O<sub>3</sub> catalyst, the above described features are similar to those observed previously by van Bokhoven and co-workers in several XAS studies after the adsorption of CO or ethene on Pt [27,30]. In these works, they explained the increase in the white-line intensity and the shift of the edge position to higher

energies as being due to the withdrawal of electron density from small platinum clusters to the adsorbed CO or ethene by means of 2π\*–d back-bond. On the other hand, XAS studies performed in the presence of H<sub>2</sub> also report similar peaks in the Δμ, this time ascribed to an induced electron transfer from Pt 6s (or 6p) orbitals to H atoms [31,32]. Based on this, the observed features in our results could be ascribed to either the presence of a π-(back)bonded (actually a combined σ and π-bonded) propene species and/or adsorbed hydrogen on Pt. Both gases are products formed during propane dehydrogenation which correlates well with the catalytic data whereby the Pt/Al<sub>2</sub>O<sub>3</sub> catalyst is initially very active for this reaction (Fig. 1). Importantly, we note that the presence of a doubly bonded (σ- and π-(back)bonded) propyl species on the Pt surface may be difficult to remove from the catalyst surface, resulting in a type of ‘product poisoning’. Such species may also readily lead to coke formation and a more permanent form of catalyst poisoning.

However, in the case of the Pt–Sn/Al<sub>2</sub>O<sub>3</sub> catalyst, no negative peak was detected in the Δμ XANES spectra. Therefore, the adsorption of hydrogen can be neglected [31,32]. The shift of the edge position to lower energies indicates that electron transfer takes place from the adsorbate to the metal. Such a phenomenon might be explained by the formation of σ-bonded Pt–propene complex, and since the Pt is electron-poor (as Sn removes charge from it), there is no additional formation of a π-back-bond. Thus, the overall Pt–propene interaction is weaker than if a sigma and pi-bonded complex forms. The IR results presented in Fig. 4 indicate that the interactions between Pt and Sn weaken the chemisorption properties of



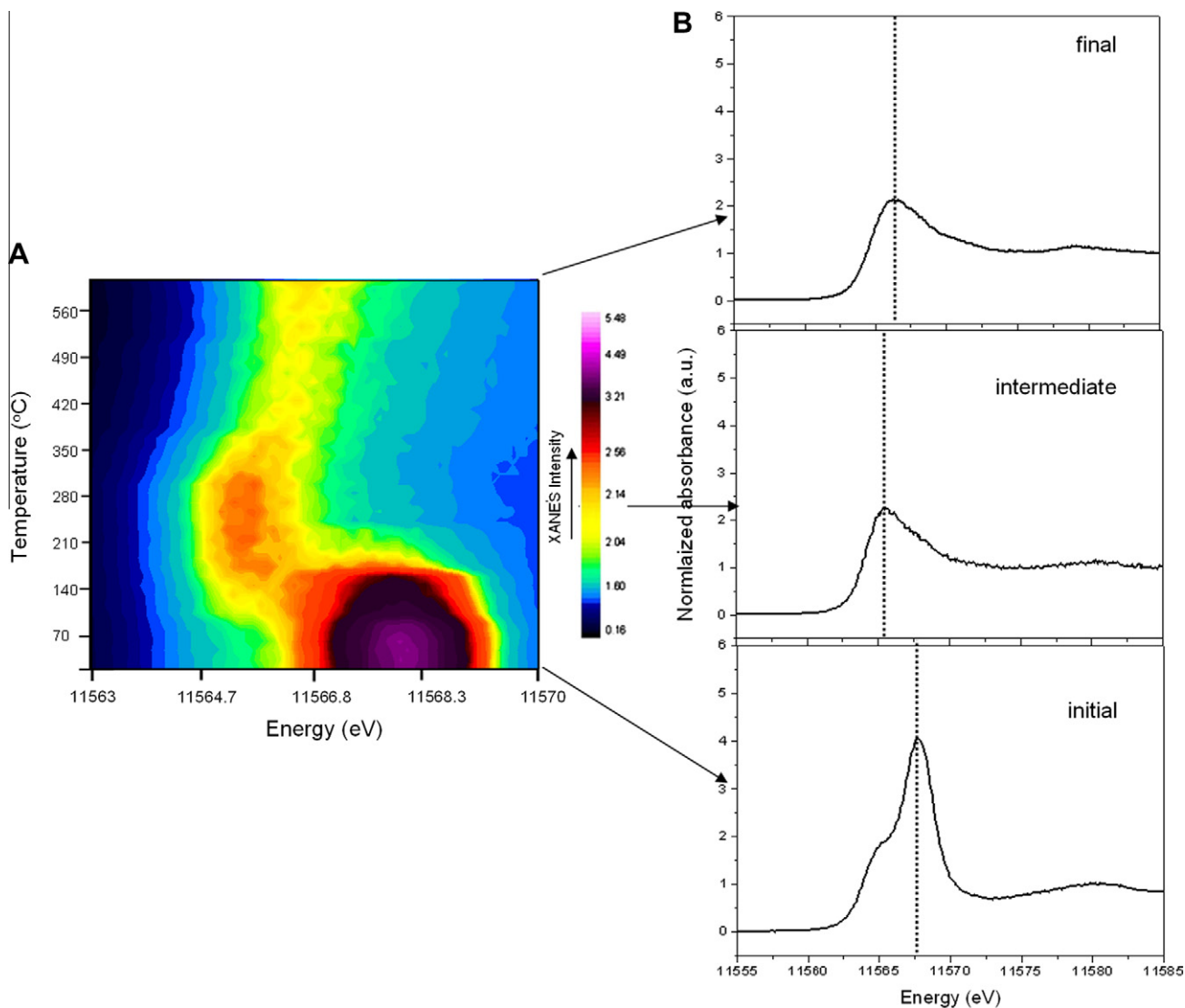


**Fig. 6.** (A) Intensity contour map of the HERFD XANES spectra of the Pt–Sn/Al<sub>2</sub>O<sub>3</sub> catalyst acquired during the ramp of temperature up 600 °C under a H<sub>2</sub> flow and (B) selection of HERFD XANES spectra of the initial, intermediate and final Pt species formed in the catalyst material.

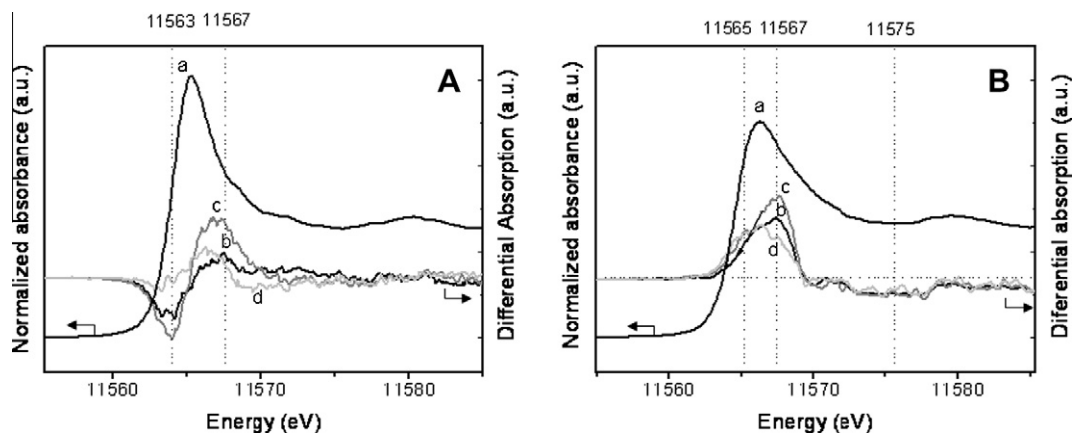


**Fig. 7.** L<sub>3</sub>-edge  $\Delta\mu$  difference XANES spectra during the ramp of temperature in propane of (A) the Pt/Al<sub>2</sub>O<sub>3</sub> catalyst at (a) 100, (b) 122 and (c) 400 °C and (B) the Pt–Sn/Al<sub>2</sub>O<sub>3</sub> catalyst at (a) 100, (b) 140 and (c) 400 °C.

Pt sites, leading to weaker interactions between the Pt sites and CO. Other works from the literature also point toward the addition of Sn to a Pt catalyst causing a reduction in the strength of interac-

tion of H<sub>2</sub>, CO and C<sub>2</sub>H<sub>2</sub> with Pt sites [28,33,34]. On other hand, a recent work [35] shows that sub-nanometer platinum clusters (Pt 8–10) as those presented here are more active and selective

than Pt surface for oxidative dehydrogenation of propane. This was explained by the attractive interaction between the under-coordinated Pt and propane. DFT calculations have shown that the initial adsorption complex between propane and the Pt cluster results in significant charge transfer from a propane C–H bonding orbital to the cluster favoring the scission of C–H bonds relative to C–C or C=C explaining the high selectivity to propene.

Accordingly, we can assume that Sn addition leads to both electronic and structural modifications of the properties of the Pt nanoparticles, which have the following implications: (i) selective C–H bond activation is favored over C–C and C=C bond rupture, leading to high selectivity to propene and (ii) coke precursors, such as (partly) dehydrogenated hydrocarbons, can easily move on the surface of Pt–Sn particles and thus they migrate from the active sites to the support before being converted by coke [20,21].

### 3.6. Study of the Pt and Pt–Sn nanoparticles behavior during consecutive dehydrogenation–regeneration cycles

The intensity contour map of the HERFD XANES spectra of the Pt/Al<sub>2</sub>O<sub>3</sub> catalyst acquired during the different treatments at the

reaction temperature of 600 °C is given in Fig. 8A. During the reaction in propane, no pronounced changes are observed. Then, after the first propane dehydrogenation reaction, the treatment in oxygen for coke burning leads to Pt entities only partially re-oxidized on the surface. The next subsequent treatment in H<sub>2</sub> to recover the active sites reduces again the Pt to metallic Pt. After this stage, the XANES spectrum possesses a more intense and better resolved white-line (Fig. 8A), indicating that sintering of the Pt nanoparticles takes place [22]. After the second cycle, the same trend is observed. In this case, partial oxidation of the Pt centers on the surface is reduced due to the bigger size of the Pt particles, which are known to be more difficult to oxidize. Therefore, in this catalyst system, successive regeneration cycles result in bigger platinum nanoparticles; this is also confirmed by the higher coordination numbers, especially after 10 cycles, as determined from the EXAFS analysis (Table 1). In Fig. 8B, we propose a general model of the Pt species present in the Pt/Al<sub>2</sub>O<sub>3</sub> catalyst at different stages of the successive (re)cycling experiment.

In the case of the Pt–Sn/Al<sub>2</sub>O<sub>3</sub> catalyst, the intensity contour map of the HERFD XANES spectra acquired during the different treatments is given in Fig. 9A. From the position and shape of

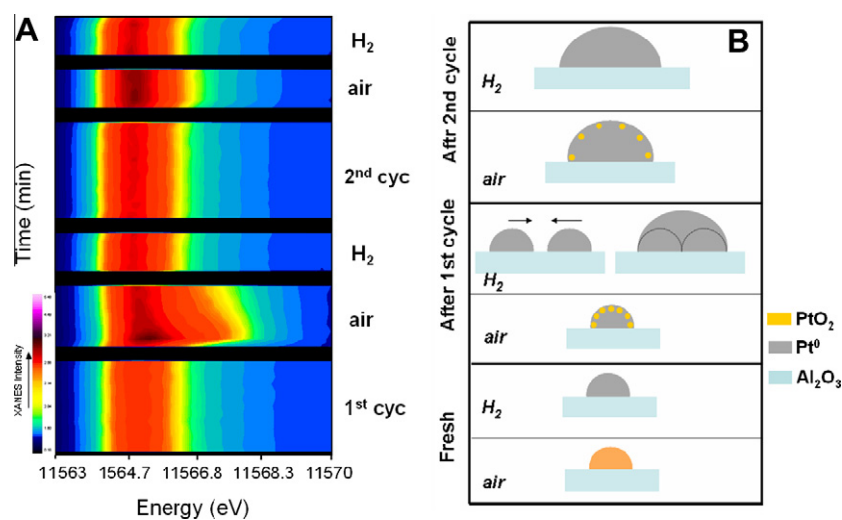


**Fig. 8.** (A) Intensity contour map of the HERFD XANES spectra of the Pt/Al<sub>2</sub>O<sub>3</sub> catalyst acquired at 600 °C during the first two propane dehydrogenation–regeneration cycles. (B) Schematic model of the Pt species during the different treatment stages for the Pt/Al<sub>2</sub>O<sub>3</sub> catalyst.

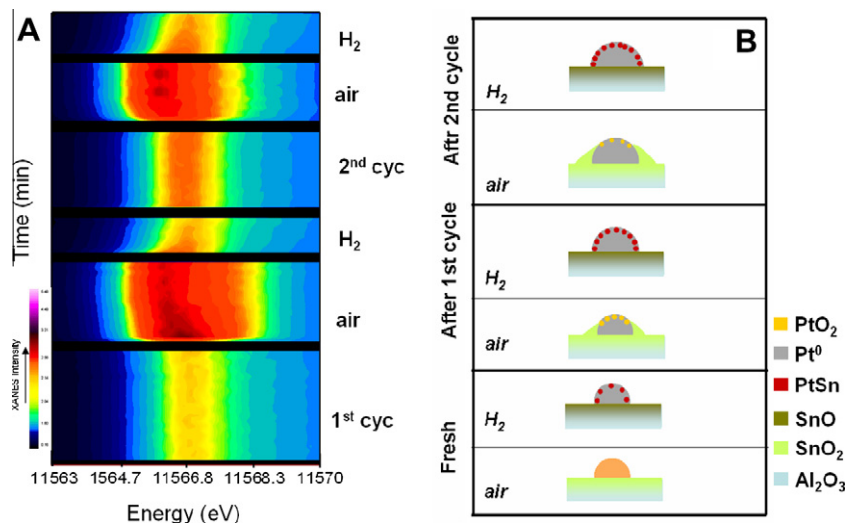


**Fig. 9.** (A) Intensity contour map of the HERFD XANES spectra of the Pt–Sn/Al<sub>2</sub>O<sub>3</sub> catalyst acquired at 600 °C during the first two propane dehydrogenation–regeneration cycles. (B) Schematic model of the Pt and Pt–Sn species during the different treatment stages for the Pt–Sn/Al<sub>2</sub>O<sub>3</sub> catalyst.

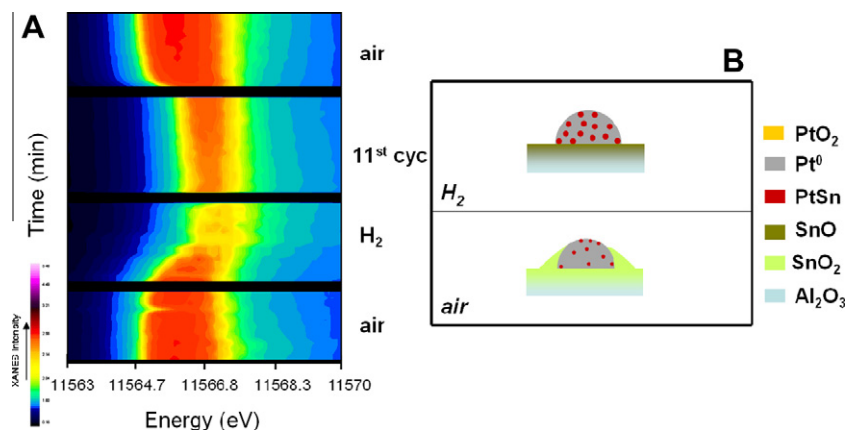


**Fig. 10.** (A) Intensity contour map of XANES spectra acquired at 600 °C during the 11th cycle for the Pt–Sn/Al<sub>2</sub>O<sub>3</sub> catalyst. (B) Schematic model of the Pt species during the different treatment stages for the Pt–Sn/Al<sub>2</sub>O<sub>3</sub> catalyst.

XANES spectra, it is clear that during the process of coke burning, oxygen oxidizes the Sn present in the Pt–Sn alloy, which segregates out of the supported Pt nanoparticles. The subsequent H<sub>2</sub> reduction restores the Pt–Sn alloy. In this catalyst material, the Pt nanoparticle size grows after the regeneration process, but the growth occurs to a lesser extent than in the Pt/Al<sub>2</sub>O<sub>3</sub> catalyst. Seemingly, the decoration of Pt particles by Sn could prevent the Pt sintering phenomenon. Fig. 9B illustrates the different stages and forms of the Pt and Pt–Sn entities during the successive propane dehydrogenation–regeneration cycling.

As a final step, the same type of experiment has been performed for the Pt–Sn/Al<sub>2</sub>O<sub>3</sub> catalyst previously subjected to 10 dehydrogenation–regeneration cycles. The results are given in Fig. 10 where it can be concluded that the variation in particle size is again rather small and that there is a Sn enrichment of the Pt–Sn alloy at the Al<sub>2</sub>O<sub>3</sub> surface.

#### 4. Conclusions

Detailed information regarding the deactivating behavior of Al<sub>2</sub>O<sub>3</sub>-supported Pt and Pt–Sn catalysts has been obtained before, during and after propane dehydrogenation and subsequent catalyst dehydrogenation–regeneration cycles under industrially relevant reaction conditions. This has been made possible by making use of a combination of complementary characterization techniques, including combined in situ UV–Vis/Raman, in situ HERFD XANES, EXAFS and CO-TPD IR spectroscopy. In particular, attention has been focused, for the first time, upon understanding the effect that multiple reaction–regeneration cycles have on the physicochemical properties of the catalyst materials. This includes the reducibility of Pt and Sn, the extent of Sn–Pt alloying, sintering of Pt nanoparticles and the surface properties of Pt. The main findings of this comprehensive study can be summarized as follows:

- (i) As a promoter, Sn has a great influence on the starting Pt phase. It reduces the average size of the Pt particles and forms an alloy with Pt. This interaction modifies the Pt electronic properties leading to more electron-poor, active particles exhibiting a higher propene turnover and improved catalytic stability;
- (ii) Sn not only modifies the electronic properties of Pt and therefore the activation of propane, but also produces a drain-off effect. The Pt L<sub>3</sub> Δμ XANES data revealed that the interaction of propane with the Pt surface appears stronger for the Pt/Al<sub>2</sub>O<sub>3</sub> catalyst than for the Pt–Sn/Al<sub>2</sub>O<sub>3</sub> catalyst leading to a partial blocking of the active site and therefore

a lower propane conversion. This may also explain the higher extent of coke formation on this catalyst material, whereas the presence of Sn keeps the Pt sites clean from coke deposits thereby increasing the catalytic stability;

- (iii) Sn segregates from the Pt–Sn alloy during coke burning, and this phenomenon could have a positive effect by stabilizing the supported Pt nanoparticles against sintering; and
- (iv) Re-activation treatments in H<sub>2</sub> are necessary in order to regenerate the active and selective Pt–Sn alloy phases. However, multiple dehydrogenation–regeneration cycles result in a gradual Sn enrichment of the alloy, which leads to a decrease in the overall dehydrogenation activity.

#### Acknowledgments

Financial support for this work comes from BASF and NRSC-Catalysis. The authors wish to acknowledge the following people for their contributions: The Sample Environment Support Service (SESS) of ESRF for providing the in situ cell for the experiments at ID26, ESRF; the beamline staff for help in the setup/data collection at DUBBLE, ESRF; Satu Korhonen and Luis Aramburo for their help during these experiments; and Matt O'Brien for his help in the Raman data processing. We also thank NWO–CW for financial support (VENI grant to AMB) and for beamtime access to the ESRF beamlines.

#### Appendix A. Supplementary material

Supplementary data associated with this article can be found, in the online version, at doi:10.1016/j.jcat.2010.09.018.

#### References

- [1] M. Eramo, Petrochemical Industry Conference Raw Materials Committee Meeting, 2004.
- [2] D. Sanfilippo, *Cattech* 4 (2000) 56–73.
- [3] D. Akporiaye, S.F. Jensen, U. Olsbye, F. Rohr, E. Rytter, M. Ronnekleiv, A.I. Spjelkavik, A. Novel, *Ind. Eng. Chem. Res.* 40 (2001) 4741–4748.
- [4] E. Rytter, H. Bolt, *CatCon2000 Proceedings*, The Catalyst Group, Spring House, PA, 2000.
- [5] H. Abrevaya, T. Imai, (UOP), US Patent 4608,360, 1986; T. Imai, (UOP), US Patent 4716,143, 1987; T. Imai, (UOP), US Patent 4762,960, 1988; T. Imai, H. Abrevaya, J.C. Bricker, D.-Y. Jan, (UOP), US Patent 4786,625, 1988.
- [6] R. Burch, A.J. Mitchell, *Appl. Catal.* 6 (1983) 121–128.
- [7] O.A. Barriás, A. Holmen, E.A. Blekkan, *Catal. Today* 24 (1995) 361–364.
- [8] J. Llorca, N. Homs, J. León, J. Sales, J.L.G. Fierro, P. Ramirez de la Piscina, *Appl. Catal. A* 189 (1999) 77–86.

- [9] C.L. Padro, S.R. de Miguel, A.A. Castro, O.A. Scelza, in: C.H. Bartholomew, G.A. Fuentes (Eds.), *Catalyst Deactivation 1997*, vol. 111, 1997, pp. 191–198.
- [10] G. Guilera, B. Gorges, S. Pascarelli, H. Vitoux, M.A. Newton, C. Prestipino, Y. Nagai, N. Hara, *J. Synchr. Rad.* 16 (2009) 628–634.
- [11] T.A. Nijhuis, S.J. Tinnemans, T. Visser, B.M. Weckhuysen, *Phys. Chem. Chem. Phys.* 5 (2003) 4361–4365; S.M. Bennici, B.M. Vogelaar, T.A. Nijhuis, B.M. Weckhuysen, *Angew. Chem. Int. Ed.* 46 (2007) 5412–5416.
- [12] A.M. Beale, B.M. Weckhuysen, *Phys. Chem. Chem. Phys.* 12 (2010) 5562–5574.
- [13] S.J. Tinnemans, M.H.F. Kox, T.A. Nijhuis, T. Visser, B.M. Weckhuysen, *Phys. Chem. Chem. Phys.* 7 (2005) 211–216.
- [14] J. Robertson, *Diamond-like amorphous carbon*, *Mater. Sci. Eng. Rep.* 37 (2002) 129–281.
- [15] F. Tuinstra, J.L. Koenig, *J. Chem. Phys.* 53 (1970) 1126–1130.
- [16] A.C. Ferrari, J. Robertson, *Phys. Rev. B* 61 (2000) 14095.
- [17] R.T. Vang, K. Honkala, S. Dahl, E.K. Vestergaard, J. Schnadt, E. Lægsgaard, B.S. Clausen, J.K. Nørskov, F. Besenbacher, *Nat. Mater.* 4 (2005) 160.
- [18] R.M. Rioux, H. Song, J.D. Hoefelmeyer, P. Yang, G.A. Somorjai, *J. Phys. Chem. B* 109 (6) (2004) 2192–2202.
- [19] M.L. Toebes, Y. Zhang, J. Hájek, T.A. Nijhuis, J.H. Bitter, A.J. van Dillen, D.Y. Murzin, D.C. Koningsberger, K.P. de Jong, *J. Catal.* 226 (2004) 215–225.
- [20] H. Lieske, A. Sárkány, J. Völter, *Appl. Catal.* 30 (1987) 69–80.
- [21] M. Santhosh Kumar, D. Chen, A. Holmen, J.C. Walmsley, *Catal. Today* 142 (2009) 17–23.
- [22] M. Fernández-García, *Catal. Rev. Sci. Eng.* 44 (2002) 59–121.
- [23] D. Bazin, D. Sayers, J.J. Rehr, C. Mottet, *J. Phys. Chem. B* 101 (1997) 5332–5336.
- [24] P. Hollins, *Surf. Sci. Rep.* 16 (1992) 51–94.
- [25] T. Visser, T.A. Nijhuis, M.J.A. van der Eerden, K. Jenken, Y. Ji, W. Bras, S. Nikitenko, Y. Ikeda, M. Lepage, B.M. Weckhuysen, *J. Phys. Chem. B* 109 (2005) 3822–3831.
- [26] M. Teliska, W.E. O’Grady, D.E. Ramaker, *J. Phys. Chem. B* 109 (2005) 8076–8084.
- [27] E. Bus, D.E. Ramaker, J.A. van Bokhoven, *J. Am. Chem. Soc.* 129 (2007) 8094–8102.
- [28] P. Biloen, F.M. Dautzenberg, W.M.H. Sachtler, *J. Catal.* 50 (1977) 77–86.
- [29] I. Lee, F. Zaera, *J. Catal.* 269 (2010) 359–366.
- [30] O.V. Safonova, M. Tromp, J.A. van Bokhoven, F.M.F. de Groot, J. Evans, P. Glatzel, *J. Phys. Chem. B* 110 (2006) 16162–16164.
- [31] K. Asakura, T. Kubota, W. Chun, Y. Iwasawa, K. Ohtani, T. Fujikawa, *J. Synchr. Rad.* 6 (1999) 439–441.
- [32] D.E. Ramaker, B.L. Mojet, M.T. Garriga Oostenbrink, J.T. Miller, D.C. Koningsberger, *Phys. Chem. Chem. Phys.* 1 (1999) 2293–2302.
- [33] R.D. Cortright, J.A. Dumesic, *J. Catal.* 148 (1994) 771–778.
- [34] H. Verbeek, W.M.H. Sachtler, *J. Catal.* 42 (1976) 257–267.
- [35] S. Vajda, M.J. Pellin, J.P. Greeley, C.L. Marshall, L.A. Curtiss, G.A. Ballentine, J.W. Elam, S. Catillon-Mucherie, P.C. Redfern, F. Mehmood, P. Zapol, *Nat. Mater.* 8 (2009) 213–216.